

# Infrared Effects of Ultraviolet Operators on Dark Matter Freeze-In

Lindsay Forestell<sup>1,2</sup> and David E. Morrissey<sup>1</sup>

<sup>1</sup>*TRIUMF, 4004 Wesbrook Mall, Vancouver, BC V6T 2A3, Canada*

<sup>2</sup>*Department of Physics and Astronomy, University of British Columbia, Vancouver, BC V6T 1Z1, Canada*

(Dated: February 28, 2022)

Dark matter (DM) that interacts too weakly with the Standard Model (SM) to reach full thermodynamic equilibrium can still be created in significant amounts by rare SM collisions. This mechanism, called freeze-in, can proceed through a renormalizable connector operator with a very small coefficient, or a non-renormalizable connector operator suppressed by a large mass scale. In the latter non-renormalizable scenario, the dominant creation of DM particles typically occurs at the largest SM temperature attained during the radiation era (assuming a standard cosmological history), and for this reason it is referred to as ultraviolet freeze-in. We show that non-renormalizable operators can also contribute importantly to the DM density at lower temperatures down to below the mass of the DM particle. To do so, we compute the production, annihilation, and freeze-out of DM in a simple dark sector consisting of a massive Dirac fermion DM candidate coupled to a massless Abelian vector boson with the only connection to the SM through the fermionic Higgs portal operator. For a broad range of parameters in the theory, the dark sector is populated by ultraviolet freeze-in in the usual way, self-thermalizes to a dark temperature below that of the SM, and undergoes thermal freeze-out. We show that late residual freeze-in reactions during the freeze-out process can further populate the dark sector and increase the DM relic density beyond standard dark sector freeze-out.

## I. INTRODUCTION

It has long been known that the Standard Model (SM) does not provide a complete description of the universe. A key missing element is dark matter (DM), which has been observed cosmologically to make up the majority of matter today [1]. However, very little is known about DM beyond its gravitational influence, such as its particle properties or how its density was created in the early universe [2–4].

Many theories of DM coupled directly to the SM rely on thermal production, with the most-studied paradigm being thermal freeze-out [5–7]. In this process, the DM species begins in thermodynamic equilibrium with the rest of the SM at temperatures above its mass. As the universe cools below the DM mass, annihilation to SM particles allows the DM density to track the exponentially suppressed equilibrium value until it becomes too slow to keep up with the cosmological expansion. This simple mechanism for DM production has many attractive features: it is insensitive to the state of the very early universe, and it yields the the correct relic abundance (to within a couple orders of magnitude) for a generic weakly-interacting massive particle (WIMP) with mass near the weak scale.

Despite these features of thermal freeze-out, the lack of discovery in direct detection experiments and collider searches for WIMPs has motivated the study of other DM production mechanisms [8, 9]. A promising alternative is freeze-in (FI) [10], in which the DM species is assumed interact only very feebly with the SM and to have an initial abundance well below the value it would obtain in equilibrium with the SM plasma. Transfer reactions of the form  $\text{SM}+\text{SM} \rightarrow \text{DM}+\text{DM}$  then create a sub-equilibrium abundance that evolves to the DM density seen today.

Within this paradigm, there are two general classes of connectors between DM and the SM with very different cosmological behaviors. The first and most studied has DM connected to the SM through a very small renormalizable operator. Production of DM for this class is dominated by temperatures near the DM mass,  $T \sim m_\psi$  [10–21]. For this reason, it is usually categorized as infrared (IR) freeze-in. This FI mechanism retains much of the attractive insensitivity to initial conditions as WIMP freeze-out aside from the assumption of a very small initial DM density. On the flip side, the renormalizable couplings needed for IR freeze-in must be extremely feeble.

The second class of connectors leading to freeze-in are non-renormalizable operators connecting the DM to the SM, whose interaction strength is naturally very small at low temperatures. Dominant DM production typically occurs at the highest SM temperatures attained during the radiation era, and for this reason they lead to what is called ultraviolet (UV) freeze-in [22–26], with a well-known example being the gravitino [27–30]. A less attractive property of this paradigm, however, is that the DM abundance depends on the state of the universe very early in its history.

In this work we demonstrate that both UV and IR freeze-in can play a role in determining the DM relic abundance through a single, non-renormalizable connector operator. This contrasts with the standard expectation that non-renormalizable operators decouple once and for all at higher temperatures. We illustrate this feature in a simple dark sector model consisting of a stable Dirac fermion  $\psi$  with mass  $m_\psi$  that is charged under an unbroken  $U(1)_x$  gauge force with vector boson  $X^\mu$  and coupling strength  $\alpha_x = g_x^2/4\pi$ . The only connection between the dark sector and the

Standard Model (SM) is assumed to be through the *fermionic Higgs portal* operator,

$$-\mathcal{L} \supset \frac{1}{M} |H|^2 \bar{\psi} \psi . \quad (1)$$

Here,  $M$  defines a very large mass scale of new physics above the energy and temperature ranges we consider. Note that we assume no gauge kinetic mixing between  $U(1)_x$  and hypercharge, which can be enforced by an exact charge conjugation symmetry in the dark sector [31].

The UV connector operator of Eq. (1) can generate both UV and IR freeze-in effects over a broad range of parameters when three plausible conditions are met. First, reheating after inflation is assumed to populate only the SM sector with visible reheating temperature  $T_{RH}$  well below the connector mass scale  $M$ . The dominant source of dark sector particles then comes from visible-to-dark transfer reactions through the connector operator (UV freeze-in). Second, for moderate to large values of the dark sector gauge coupling  $\alpha_x$  the dark sector can self-thermalize to a temperature  $T_x$  less than the visible temperature  $T$  but greater or similar to the dark fermion mass  $m_\psi$ . And third, if the DM annihilation cross section is sufficiently large the DM abundance can track the equilibrium abundance (at temperature  $T_x < T$ ) for long enough that transfer reactions from the non-renormalizable connector operator return as the dominant contributor to the DM abundance. To the best of our knowledge, combined UV and IR freeze-in effects have not been investigated before, and they provide a counterexample to the standard decoupling of non-renormalizable operators in the early universe.

The combined UV and IR freeze-in behavior we focus on in the present work is only one of a number of “phases” of freeze-out and freeze-in possible within this simple dark sector model. These phases are analogous to the four phases studied in Ref. [14] for a similar dark sector consisting of a charged complex scalar DM particle connected to the SM Higgs field through the standard renormalizable Higgs portal operator, but tilted towards the UV. When the mass scale  $M$  in the fermionic connector operator of Eq. (1) is large relative to the weak scale and  $\alpha_x \rightarrow 0$ , the theory reduces to standard UV freeze-in of  $\psi$  dark matter as studied in Ref. [24] with no significant dark self-thermalization or later annihilation. In contrast, for much smaller  $M$  near the TeV scale the dark and visible sectors are thermally coupled (via the connector) throughout  $\psi$  freeze-out, and this operator can control the freeze-out process even when  $\alpha_x$  is very small [32–34]. We focus on the scenario between these relative extremes with larger  $M$  and  $\alpha_x$ .

This paper is structured as follows. Following the introduction, we discuss in Sec. II the UV freeze-in transfer of number and energy density through the connector operator of Eq. (1) as well as dark self-thermalization. Next, in Sec. III we compute the interplay between freeze-out and IR freeze-in in determining the relic abundance  $\psi$  particles and determine the conditions under which both UV and IR freeze-in can be relevant. In Sec. IV, we comment briefly on the astrophysical implications of the new dark force from dark matter self-interactions. Finally, Sec. V is reserved for our conclusions. Some technical details related to thermally-averaged cross sections are contained in Appendix A.

## II. POPULATING THE DARK SECTOR THROUGH UV FREEZE-IN

We begin by investigating the transfer of energy and number density to the dark sector by UV freeze-in through the connector operator of Eq. (1). For this, we make the standard freeze-in assumption that only the visible SM sector is populated significantly by reheating after inflation with reheating temperature  $T_{RH} \ll M$  [10, 22].<sup>1</sup> The dark sector is then populated by transfer reactions of the form  $H + H^\dagger \rightarrow \psi + \bar{\psi}$  (assuming unbroken electroweak) mediated by the operator of Eq. (1). Once the number density of  $\psi$  grows large enough, the dark sector may also thermalize to an effective temperature  $T_x$  through further reactions such as  $\psi + \bar{\psi} \leftrightarrow X^\mu + X^\nu$ . In this section we study the creation of  $\psi$  particles from SM collisions during and after reheating as well as the conditions for the self-thermalization of the dark sector.

### A. Transfer without the Dark Vector

It is convenient to study first the creation of  $\psi$  fermions by SM collisions in the absence of dark vectors ( $\alpha_x \rightarrow 0$ ) [24]. The number and energy transfer via  $H + H^\dagger \rightarrow \psi + \bar{\psi}$  is described by

$$\frac{dn_\psi}{dt} = -3Hn_\psi - \langle \sigma_{tr} v(T) \rangle (n_\psi^2 - n_{\psi,eq}^2(T)) \quad (2)$$

$$\frac{d\rho_x}{dt} = -3H\rho_x - \langle \Delta E \cdot \sigma_{tr} v(T) \rangle (n_\psi^2 - n_{\psi,eq}^2(T)) \quad (3)$$

where  $\rho_x$  is the total energy density in the dark sector and  $\Delta E$  is the energy transfer per collision.

Starting with number transfer, in the limit of  $n_\psi \ll n_{\psi,eq}$  and  $T \gg m_\psi$  the collision term is approximately

$$-\langle \sigma_{tr} v(T) \rangle (n_\psi^2 - n_{\psi,eq}^2(T)) \simeq \frac{1}{4\pi^5} \frac{T^6}{M^2}. \quad (4)$$

Details of the calculation are given in Appendix A. Assuming radiation domination up to the reheating temperature  $T_{RH} \gg m_\psi$ , this gives the simple solution for the yield of  $\psi$  (and  $\bar{\psi}$ ) of

$$Y_\psi(T) \simeq Y_\psi(T_{RH}) + Y_{\psi,eq}(T) \frac{\sqrt{5/2}}{2\zeta(2)\pi^4} g_*^{-1/2} \frac{M_{\text{Pl}} T_{RH}}{M^2} \left[ 1 - \left( \frac{T_{RH}}{T} \right)^{-1} \right]. \quad (5)$$

This solution only holds in the limit  $Y_\psi \ll Y_{\psi,eq}$ , corresponding to a consistency condition of (for  $Y_\psi(T_{RH}) \rightarrow 0$  and  $T \ll T_{RH}$ )<sup>2</sup>

$$T_{RH} \ll \frac{2\zeta(2)\pi^4}{\sqrt{5/2}} g_*^{1/2} \frac{M^2}{M_{\text{Pl}}}. \quad (6)$$

<sup>1</sup> Obtaining such an asymmetric reheating between different sectors has been studied recently in Refs. [35, 36].

<sup>2</sup> The number and energy density produced through thermal transfer prior to reheating by the operator of Eq. (1) is a very small fraction of that produced at reheating [24, 25].

Larger reheating temperatures imply thermalization between the dark and visible sectors at reheating with  $Y_\psi(T) \rightarrow Y_{\psi,eq}(T)$  for  $T \sim T_{RH}$ . In this work we focus on the non-thermalization scenario.

Turning next to energy transfer, the transfer term is computed in Appendix A and for  $m_\psi \ll T \ll M$  and  $n_\psi \ll n_{\psi,eq}$  reduces to

$$-\langle \Delta E \cdot \sigma_{tr} v(T) \rangle (n_\psi^2 - n_{\psi,eq}^2(T)) \simeq \frac{3}{2\pi^5} \frac{T^7}{M^2}. \quad (7)$$

Solving as above, we find

$$\left( \frac{\rho_x}{\rho_{\psi,eq}} \right) \simeq \left( \frac{\rho_x}{\rho_{\psi,eq}} \right)_{T_{RH}} + \frac{180\sqrt{10}}{7\pi^8} g_*^{-1/2} \frac{M_{\text{Pl}} T_{RH}}{M^2} \left[ 1 - \left( \frac{T_{RH}}{T} \right)^{-1} \right]. \quad (8)$$

Again, this is only valid for  $Y_\psi \ll Y_{\psi,eq}$ . For sufficiently large  $T_{RH}$ ,  $\rho_x \rightarrow \rho_{\psi,eq}(T)$  at  $T \sim T_{RH}$ .

Comparing  $Y_\psi$  and  $\rho_x$  found above for  $Y_\psi \ll Y_{\psi,eq}$ , we see that the mean momentum of the fermions produced near reheating is on the order  $p \sim T_{RH}$ . At later times, these momenta simply redshift as  $1/a$  provided  $T \gg m_\psi$ . Indeed, the detailed analysis of Ref. [24] shows that (in the absence of dark vectors) the dark fermions obtain an approximate *Bose-Einstein* distribution with effective temperature  $T_x \simeq (1.155) T_{RH}(a_{RH}/a)$ .

## B. Thermalization with the Dark Vector

Let us now include a dark vector boson  $X^\mu$  coupling to  $\psi$  with strength  $\alpha_x = g_x^2/4\pi$ . This interaction allows the dark fermions to scatter with each other, annihilate to vector bosons, and emit vectors as radiation. If these reactions are strong enough, the dark fermion and vector species can thermalize with each other to yield an effective temperature  $T_x \leq T$ .

The self-thermalization of heavy dark particles coupled to a massless dark vector was investigated in Refs. [14, 26]. As in these works, we only make parametric estimates of the very complicated full thermalization processes. We identify self-thermalization in the dark sector with the condition

$$\Gamma_{th}(T_{th}) = H(T_{th}), \quad (9)$$

where  $\Gamma_{th}$  is an effective thermalization rate to be discussed below and this relation defines the visible thermalization temperature  $T_{th}$  implicitly. Note that  $T_{th} \leq T_{RH}$ , and we set  $T_{th} = T_{RH}$  if  $\Gamma_{th}(T_{RH}) \geq H(T_{RH})$ .

It is convenient to classify the thermalization processes contributing to  $\Gamma_{th}$  into: i)  $2 \rightarrow 2$  processes with hard momentum exchange; ii)  $2 \rightarrow 3$  inelastic processes together with  $2 \rightarrow 2$  with soft momentum exchange. The first class includes annihilation  $\psi + \bar{\psi} \rightarrow X^\mu + X^\nu$  and hard scatterings such as  $\psi + \psi \rightarrow \psi + \psi$  for which we estimate the rate to be [14]

$$\Gamma_{el}(T) \sim \frac{\pi \alpha_x^2}{T^2} n_\psi(T), \quad (10)$$

where  $n_\psi(T)$  is the number density of  $\psi$  prior to dark self-thermalization. Using Eq. (5) (with  $Y_\psi(T_{RH}) \rightarrow 0$ ), for  $T \gg m_\psi$  it is given by

$$n_\psi(T) \simeq \frac{3\sqrt{5/2}}{2\pi^6 g_*^{1/2}} \frac{M_{\text{Pl}} T_{RH}}{M^2} T^3. \quad (11)$$

The second class of soft and inelastic processes was studied in Ref. [26] with the net result

$$\Gamma_{in}(T) \sim \min \left\{ \frac{\alpha_x^3 n_\psi(T)}{\mu_{IR}^2}, \alpha_x^2 \sqrt{n_\psi/T} \right\}, \quad (12)$$

where  $\mu_{IR}$  an effective infrared cutoff given by

$$\mu_{IR} = \max \left\{ \sqrt{\alpha_x n_\psi/T}, H, m_\psi \right\}. \quad (13)$$

We take the full thermalization rate to be the sum of the hard and inelastic rates,  $\Gamma_{th} = \Gamma_{in} + \Gamma_{el}$ .

If thermalization occurs with  $T_{th} \gg m_\psi$ , a smaller number of  $\psi$  and  $\bar{\psi}$  fermions with typical energy  $T$  are redistributed into a larger number of  $\psi$ ,  $\bar{\psi}$ , and  $X^\mu$  particles in equilibrium with each other at temperature  $T_x$ . Treating the thermalization as instantaneous, the resulting dark sector temperature can be obtained from energy conservation and the result of Eq. (8):

$$\frac{T_x(T_{th})}{T_{th}} \equiv \xi(T_{th}) \simeq \left[ \frac{180\sqrt{10}}{11\pi^8 g_*^{1/2}} \frac{M_{\text{Pl}} T_{RH}}{M^2} \right]^{1/4}. \quad (14)$$

At later times, separate conservation of entropy in the dark and visible sectors implies

$$\xi(T) \simeq \xi(T_{th}) \left[ \frac{g_{*S}(T)}{g_{*S}(T_{th})} \cdot \frac{g_{*S,x}(T_{th})}{g_{*S,x}(T)} \right]^{1/3}, \quad (15)$$

where  $g_{*S(x)}$  refers to the number of visible (hidden) entropy degrees of freedom.

The analysis leading to the temperature ratio of Eq. (14) has three assumptions built into it, and their consistency implies maximal and minimal allowed values of  $\xi(T_{th})$ . First, the assumption of non-thermalization between the visible and dark sectors implies  $\xi(T_{th}) \ll 1$ . Second, the validity of the effective connector operator description of Eq. (1) requires  $T_{RH} \ll M$  corresponding to a maximum value of  $\xi(T_{th}) \lesssim (10^{-3} M_{\text{Pl}}/M)^{1/4}$ . And third, we have so far neglected the mass of the  $\psi$  fermion. Demanding that  $T_x(T_{th}) \gtrsim m_\psi$  then leads to a lower bound on  $\xi(T_{th})$  that we use to define

$$\xi_{min} \equiv \frac{m_\psi}{T_{th}}. \quad (16)$$

This also defines an implicit lower bound on the thermalization temperature for given values of  $m_\psi$ ,  $M$ , and  $\alpha_x$ , and correspondingly a lower limit on the reheating temperature  $T_{RH}$ .

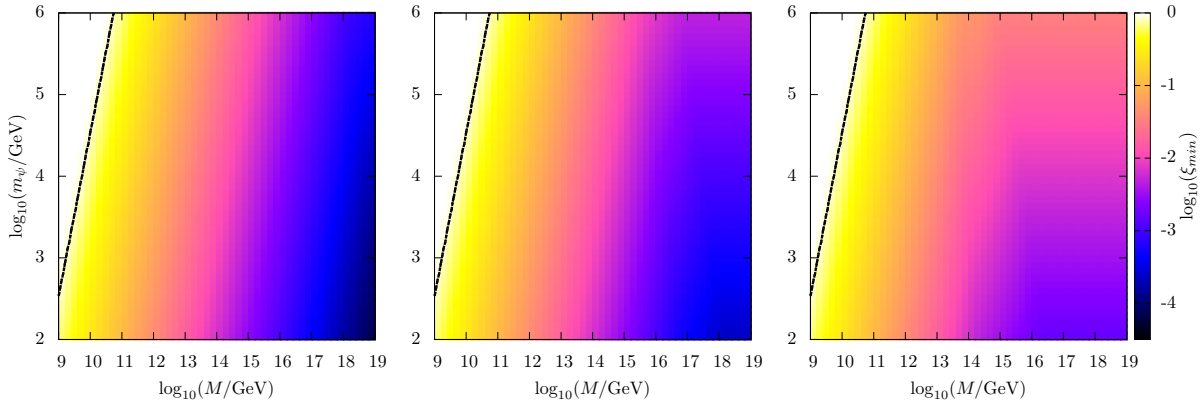


FIG. 1. Minimum consistent values of  $\xi(T_{RH})$  in the  $M$ – $m_\psi$  plane for  $\alpha_x = 10^{-1}$  (left),  $10^{-2}$  (middle),  $10^{-3}$  (right). The black line indicates where  $\xi(T_{RH}) \rightarrow 1$  and our assumption of non-thermalization with the SM breaks down.

In Fig. 1 we show the values of  $\xi_{min}$  in the  $M$ – $m_\psi$  plane for  $\alpha_x = 10^{-1}$  (left),  $10^{-2}$  (middle), and  $10^{-3}$  (right). Larger  $M$  and  $\alpha_x$  and smaller  $m_\psi$  lead to smaller  $\xi_{min}$ . The white regions in the upper left corners of the plots (bounded by black lines) have  $\xi_{min} \rightarrow 1$  corresponding to thermalization between the visible and dark sectors when dark self-thermalization is achieved. As stated above, in the analysis to follow we focus on the lower right region where this does not occur.

### III. FREEZE-OUT AND LATE TRANSFER IN THE DARK SECTOR

If the dark sector is populated by UV freeze-in and is self-thermalized at temperature  $T_x \gtrsim m_\psi$ , the dark fermion will undergo freeze-out by annihilation to dark vectors when  $T_x$  falls below  $m_\psi$ . While freeze-out in a dark sector with  $T_x \ll T$  has been studied in Refs. [26, 37–39], we point out a qualitatively new feature in the present context. Specifically, we show that the UV connector operator responsible for initially populating the dark sector at reheating can drastically change the freeze-out dynamics at much later times.

#### A. Evolution Equations

The evolution of the  $\psi$  dark fermion number density at  $T_x \lesssim m_\psi$  is described by

$$\frac{dn_\psi}{dt} + 3H n_\psi \simeq - \langle \sigma v(T_x) \rangle_{ann} (n_\psi^2 - n_{\psi,eq}^2(T_x)) + \langle \sigma_{tr} v(T) \rangle n_{\psi,eq}^2(T) \quad (17)$$

In writing this expression we have assumed self-thermalization in the dark sector with  $T_x \ll T$  and no asymmetry between  $\psi$  and  $\bar{\psi}$ .

The first term on the right side of Eq. (17) describes annihilation  $\psi + \bar{\psi} \rightarrow X^\mu + X^\nu$  with a thermal average at temperature  $T_x$ . The leading-order perturbative result for the cross section at

low velocity is [40]

$$\sigma_{ann,p}v = \frac{\pi \alpha_x^2}{m_\psi^2} . \quad (18)$$

However, the full cross section receives independent non-perturbative enhancements from the Sommerfeld effect [41–43] and bound state formation [37, 44]. The full cross section can be written in the form [37, 45]

$$\sigma_{ann}v = [\mathcal{S}_{somm}(v) + \mathcal{S}_{rec}(v)] \sigma_{ann,p}v , \quad (19)$$

where  $v$  is the relative velocity and

$$\mathcal{S}_{somm}(v) = \frac{2\pi z}{1 - e^{-2\pi z}} , \quad (20)$$

$$\mathcal{S}_{rec}(v) = \mathcal{S}_{somm}(v) \frac{2^9}{3} \frac{z^4}{(1+z^2)^2} e^{-4z \tan^{-1}(1/z)} , \quad (21)$$

with  $z = \alpha_x/v$ , and which have the limits  $\mathcal{S}_i(v) \rightarrow 1$  for  $v \gg \alpha_x$ .

The second term on the right side of Eq. (17) corresponds to transfer reactions of the form  $H + H^\dagger \rightarrow \psi + \bar{\psi}$ , and has all relevant quantities evaluated at the visible temperature  $T$ .<sup>3</sup> An explicit expression for this transfer term is given in Appendix A, which reduces to

$$\langle \sigma_{tr,v}(T) \rangle n_{\psi,eq}^2(T) \equiv \mathcal{T}(T) \simeq \begin{cases} \frac{1}{4\pi^5} \frac{T^6}{M^2} & ; T \ll m_\psi \\ \frac{3}{32\pi^4} \frac{m_\psi^2 T^4}{M^2} e^{-2m_\psi/T} & ; T \gg m_\psi \end{cases} . \quad (22)$$

For  $T_x < m_\psi$  but  $T \gg m_\psi$ , the annihilation term in Eq. (17) receives an exponential suppression in temperature while the transfer term is only suppressed by a power. We show below that this can allow the transfer term derived from a UV connector operator to play a significant role in the IR.

## B. Analytic Estimates

It is instructive to estimate the relic density of  $\psi$  particles analytically to understand the effect of late-time transfer by the UV connector. To do so, we treat the annihilation cross section as being power-law in velocity:  $\langle \sigma_{ann}v \rangle \rightarrow \sigma_0 x_x^{-n}$  where  $x \equiv m_\psi/T$  and  $x_x \equiv m_\psi/T_x = \xi^{-1} x$ .

### Freeze-Out Without the Transfer Term

<sup>3</sup> Since  $T_x \ll T$ , we can neglect the reverse reaction.



Consider first the relic density of  $\psi$  with no transfer term but a definite value of  $\xi \ll 1$ . This can be computed by a simple generalization [37–39] of the analytic freeze-out approximation of Refs. [5–7, 46, 47]. Freeze-out occurs when the mass to dark temperature ratio is

$$x_{x,fo} \simeq \ln \left[ (0.192)(n+1)(g_\psi/g_*^{1/2})M_{\text{Pl}} m_\psi \sigma_0 \xi^2 \right] - (n + \frac{1}{2}) \ln(x_{x,fo}) , \quad (23)$$

which can be solved iteratively for  $x_x^{fo}$ . This translates into an approximate relic density of<sup>4</sup>

$$\Omega_\psi h^2 \simeq (2.07 \times 10^8 \text{ GeV}^{-1}) \frac{\xi (n+1) x_{x,fo}^{n+1}}{(g_{*S}/g_*^{1/2})M_{\text{Pl}} \sigma_0} . \quad (24)$$

Relative to the freeze-out of a species in thermodynamic equilibrium with the visible sector with the same mass and cross section, these relations imply

$$x_x^{fo} \simeq \tilde{x}^{fo} + (2 - 1/\tilde{x}_{fo}) \ln \xi , \quad \Omega_\psi h^2 \simeq \xi \left( 1 + 2 \ln \xi / \tilde{x}^{fo} \right) \tilde{\Omega}_\psi h^2 , \quad (25)$$

where  $\tilde{x}^{fo}$  and  $\tilde{\Omega}_\psi h^2$  are the values for these quantities if the species were thermally coupled to the SM. The most important change is a reduction of the relic density by a factor of about  $\xi \ll 1$ .

### Freeze-Out With the Transfer Term

Let us now include the transfer term from Eq. (17) in the evolution of the density of  $\psi$ . As  $T_x$  falls below  $m_\psi$ , annihilation is expected to dominate and keep  $n_\psi$  close to its equilibrium value at temperature  $T_x$ . However, since the corresponding annihilation rate falls exponentially in this regime, it decreases more quickly than the Hubble and transfer rates, and thus the near-equilibrium regime ends when one of these other rates catches up. We show here that late-time transfer reactions can significantly modify the final  $\psi$  relic density when the annihilation rate meets the transfer rate before reaching Hubble.

Define  $T_{x,=}$  to be the value of the dark temperature  $T_x$  that solves the equation

$$\langle \sigma_{ann} v(T_x) \rangle n_{\psi,eq}^2(T_x) = \mathcal{T}(T_x/\xi) , \quad (26)$$

where  $\mathcal{T}(T)$  is the transfer rate given in Eq. (22). If the solution has  $T_+ = T_{x,=}/\xi < m_\psi$ , an approximate expression for it is

$$x_{x,=} \simeq \frac{1}{2} \ln \left( \frac{\pi^2}{2} g_\psi^2 \sigma_0 M^2 \xi^6 \right) + \left( \frac{3-n}{2} \right) \ln(x_{x,=}) , \quad (27)$$

which can be solved iteratively for  $x_{x,=}$  provided it is greater than unity. When  $x_{x,=}$  is greater than the freeze-out temperature without transfer,  $x_{x,fo}$  given in Eq. (23), the transfer operator does not

---

<sup>4</sup> Note that we use  $M_{\text{Pl}} = 2.43 \times 10^{18}$  GeV, and the full DM relic density is the sum of equal  $\psi$  and  $\bar{\psi}$  densities.

significantly alter the  $\psi$  relic density. In particular, the condition  $x_{x,=} > x_{x,fo}$  implies that the evolution of the  $\psi$  density is dominated by Hubble dilution rather than transfer for all  $x_x > x_{x,fo}$  since the expansion term decreases less quickly than the transfer term in this regime. In contrast, transfer effects are important for  $x_{x,=} < x_{x,fo}$ .

When  $x_{x,=} < x_{x,fo}$ , the transfer and annihilation terms in Eq. (17) can reach a balance with each other for  $x_x > x_{x,=}$  until the Hubble term catches up. The number density of  $\psi$  is then approximately

$$n_{\psi,=(T_x)} \simeq \sqrt{\frac{\mathcal{T}(T_x/\xi)}{\sigma_0}} x_x^{n/2} \quad (28)$$

$$\rightarrow \frac{1}{2\pi^{5/2}} \frac{m_\psi^3}{\sqrt{\sigma_0 M^2}} \xi^{-3} x_x^{-3+n/2} \quad (T_x/\xi \gg m_\psi) \quad (29)$$

where the expression in the second line only applies for  $T_x/\xi \gg m_\psi$ . Note that the density in this regime is always greater than the equilibrium density  $n_{\psi,eq}(T_x)$ , even when  $T_x/\xi < m_\psi$ .

If the balance regime is achieved,  $x_{x,=} < x_{x,fo}$ , it ends when the Hubble term in Eq. (17) catches up to the annihilation and transfer terms. This later decoupling corresponds approximately to the condition

$$\langle \sigma_{ann} v(T_x) \rangle n_{\psi,=(T_x)} \simeq H(T_x/\xi) . \quad (30)$$

Defining  $T_{x,dec}$  as the dark temperature that satisfies the relation above, an approximate solution for  $T_{x,dec}/\xi \gg m_\psi$  is

$$x_{x,dec} \simeq \left[ (0.086) \frac{m_\psi M_{\text{Pl}} \sqrt{\sigma_0}}{g_*^{1/2} M} \xi^{-1} \right]^{1/(1+n/2)} . \quad (31)$$

The solution for  $T_{x,dec}/\xi \lesssim m_\psi$  is more complicated but can be obtained similarly. The final relic density can be written in a form very similar to standard freezeout via Eq. (30):

$$\Omega_\psi h^2 \simeq (2.07 \times 10^8 \text{ GeV}^{-1}) \frac{\xi x_{x,dec}^{n+1}}{(g_{*S}/g_*^{1/2}) M_{\text{Pl}} \sigma_0} . \quad (32)$$

Since  $n_{\psi,=(T_x)} > n_{\psi,eq}(T_x)$  we must have  $x_{x,dec} > x_{x,fo}$  whether or not  $T_{x,dec}/\xi$  is larger or smaller than  $m_\psi$ , and therefore the relic density of Eq. (32) is bigger than the pure freeze-out result of Eq. (24).

### C. Numerical Results for Freeze-Out

To confirm the analytic estimates derived above and map out the parameter space of theory, we perform a full numerical analysis of the dark matter freeze-out process. In Fig. 2 we show

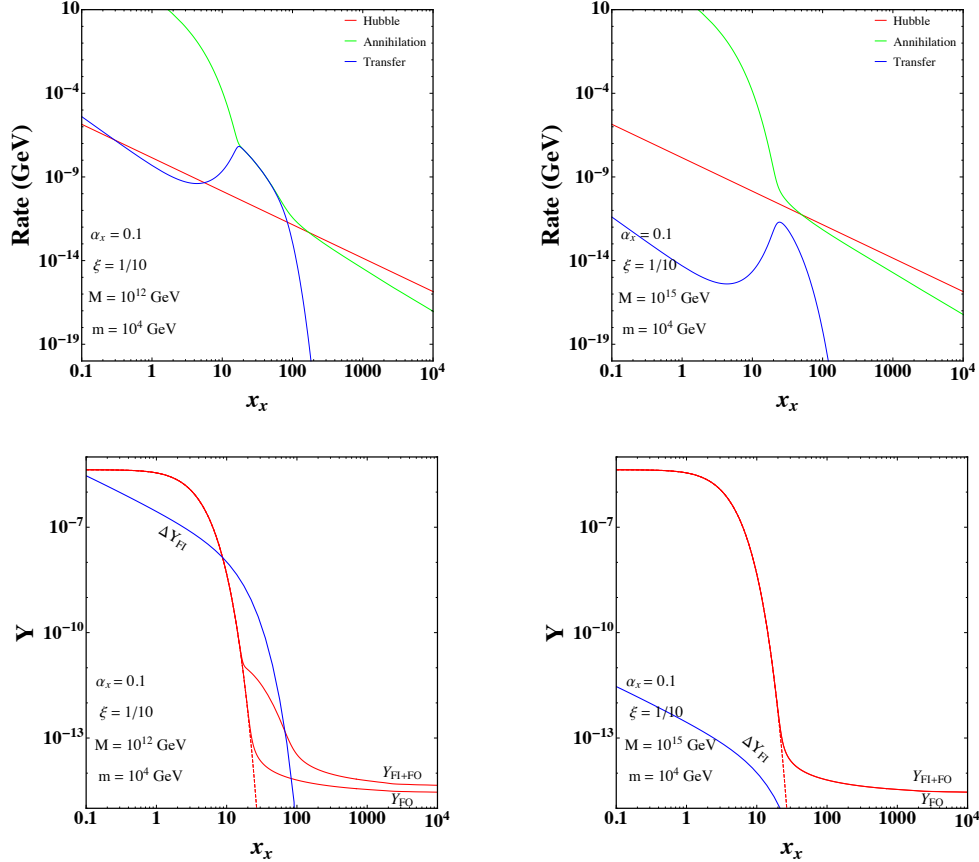


FIG. 2. Evolution of the relevant rates in the upper panels and the  $\psi$  density in the lower panels for  $\alpha_x = 0.1$ ,  $\xi = 0.1$ ,  $m_\psi = 10^4$  GeV, and  $M = 10^{12}$  GeV (left) and  $10^{15}$  GeV (right).

the evolution of the relevant rates in the upper panels and the  $\psi$  density in the lower panels for  $\alpha_x = 0.1$ ,  $\xi = 0.1$ ,  $m_\psi = 10^4$  GeV, and  $M = 10^{12}$  GeV (left) and  $10^{15}$  GeV (right). The rate plots show the rates for Hubble, annihilation, and late transfer defined according to

$$\text{Hubble} = H(T), \quad \text{Annihilation} = \langle \sigma_{ann} v(T_x) \rangle n_\psi, \quad \text{Transfer} = \mathcal{T}(T)/n_\psi, \quad (33)$$

where  $n_\psi$  is the number density obtained from solving Eq. (17) and  $\mathcal{T}(T)$  is the transfer rate of Eq. (22). The value of  $M$  is smaller in the left panels of this figure, and late-time transfer In the  $\psi$  number density plots, we show the densities in equilibrium (dashed line), and with and without the transfer operator (upper and lower solid lines).

Late transfer by the fermionic Higgs portal operator is seen to increase significantly the final relic density in the left panels of Fig. 2, while its effect is negligible in the right panels. The difference corresponds to the larger transfer rate for  $M = 10^{12}$  GeV in the left panels versus  $M = 10^{15}$  GeV in the right. Following the rates for  $M = 10^{12}$  GeV, transfer is seen to catch up to annihilation before Hubble leading to a regime of balanced rates and enhanced number density. In contrast, the Hubble rate catches up to annihilation before transfer in the right panels with  $M = 10^{15}$  GeV and never plays a significant role in the evolution of  $n_\psi$ .

In Fig. 3 we show the enhancement of the relic density in the  $M$ - $m_\psi$  plane for  $\alpha_x = 0.1$  (left)

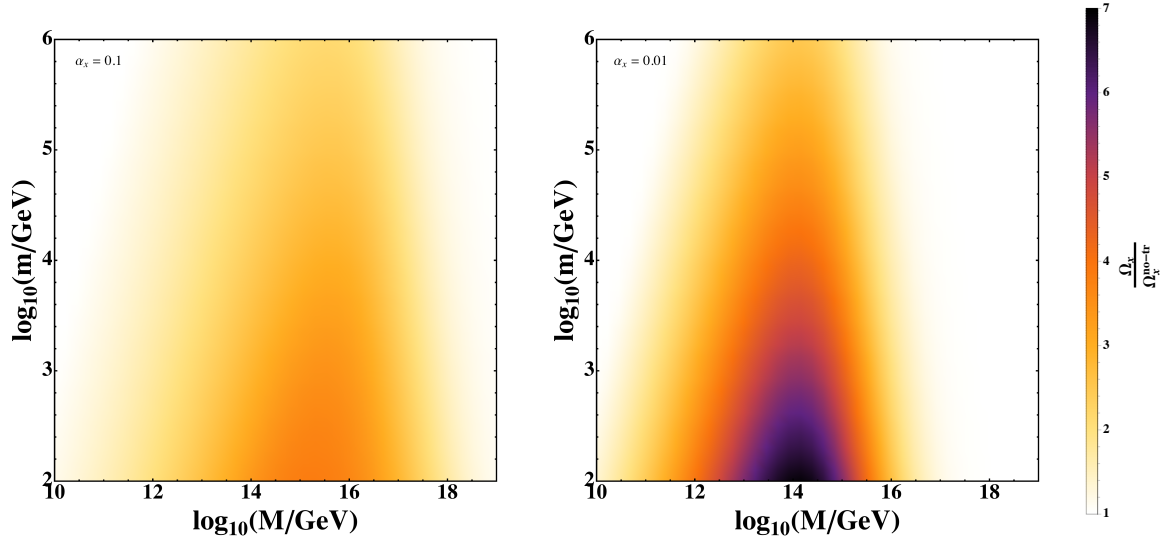


FIG. 3. Enhancement of the  $\psi$  relic density due to late transfer effects relative to the value without this effect,  $\Omega_\psi/\Omega_\psi^{no-tr}$  for  $\alpha_x = 0.1$  (left) and  $0.01$  (right) and  $\xi = \xi_{min}$ .

and  $0.01$  (right) with  $\xi = \xi_{min}$  as computed previously. The contours in both panels indicate the relic density we find to the value that would be obtained without late transfer effects,  $\Omega_\psi/\Omega_\psi^{no-tr}$ . Late transfer by the connector operator initially increases as  $M$  decreases and the transfer operators becomes more effective. However, as  $M$  continues to decrease we find a competing effect between the efficiency of transfer and the increasing value of  $\xi_{min}$ . As the dark and visible temperatures approach each other, transfer is more likely to occur while  $T \rightarrow m_\psi$  and the effect becomes exponentially suppressed, as seen in Eq. (22). Transfer effects are also reduced at  $\alpha_x = 0.1$  relative to  $\alpha_x = 0.01$  due to the non-perturbative enhancements in the annihilation cross section at low velocities for the larger value of the gauge coupling.

Ultimately, we are interested in the parameter space where  $\psi$  can make up all the dark matter. In Fig. 4 we show the values of  $m_\psi$  for which this occurs as a function of  $M$  for  $\alpha_x = 0.1$  (left) and  $0.01$  (right) for various values of  $\xi$  (solid lines). The lines in these plots are cut off at smaller  $M$  when  $\xi$  falls below  $\xi_{min}$ . As expected from the annihilation cross section, larger values of  $\alpha_x$  coincide with larger dark matter masses. In the right part of both panels the allowed DM mass  $m_\psi$  reaches a value that is independent of  $M$  for fixed  $\xi$ . This region corresponds to late transfer being negligible for the freeze-out process, with the relic density scaling approximately as  $\xi^{-1}\alpha_x^2/m_\psi^2$ . Going to smaller  $M$ , transfer eventually becomes important and the relic density increases. Correspondingly, the mass  $m_\psi$  that produces the correct relic density decreases. As  $M$  decreases further, the lines for different  $\xi$  values in Fig. 4 come together. This can be understood from Eqs. (31) and (32), where the direct dependence on  $\xi$  is seen to cancel for cross sections  $\langle\sigma_{ann}v\rangle = \sigma_0 x^{-n}$  with  $n \rightarrow 0$ , as we have here (up to the Sommerfeld and bound state enhancements). The upper shaded region in both panels is excluded because the resulting relic density of  $\psi$  is always greater than the observed DM density for any consistent value of  $\xi$ . Going from  $\alpha_x = 0.1$  to  $0.01$ , lower  $\psi$  masses are needed to produce the correct relic density. Also shown in this figure are bounds from DM self-interactions to be discussed below.

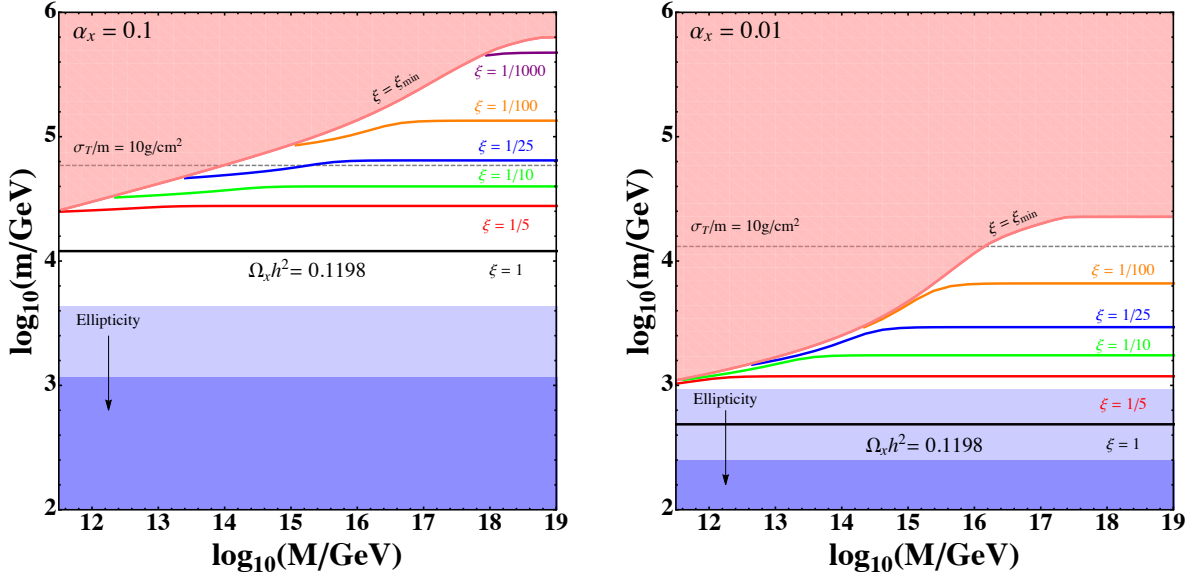


FIG. 4. Values of  $m_\psi$  that give the correct relic density of  $\psi$  dark matter as a function of  $M$  for  $\alpha_x = 0.1$  (left) and  $0.01$  (right) for various fixed values of  $\xi$ . Each solid line corresponds to the correct  $\psi$  relic density for the corresponding value of  $\xi$ . The red shaded upper region is excluded due to overproduction of  $\psi$  relic density for any consistent value of  $\xi$ . The lower blue shaded regions indicate exclusions from the effects of  $\psi$  dark matter self-interactions from the observed ellipticity of galactic halos, with the dark blue indicating a conservative exclusion and the light blue showing a more aggressive one. The dotted line indicates a DM self-scattering transfer cross-section per mass in dwarf halos of  $\sigma_T/m_\psi = 10 \text{ cm}^2/\text{g}$ .

#### IV. DARK MATTER SELF-INTERACTIONS

Dark matter in our theory is charged under an unbroken  $U(1)_x$  gauge force implying long-range self interactions among DM particles that can modify their behavior in collapsed systems. Such interactions have been suggested as a way to resolve several apparent discrepancies between simulations of DM structure formation and observations [48, 49]. However, these interactions are also constrained to not be so large as to overly disrupt cosmic structures [50, 51].

An upper bound on DM self-interactions can be derived from the observed ellipticity of galactic halos such as NGC720 [52, 53]. For charged DM coupled to an unbroken  $U(1)$ , Refs. [37, 39] derived limits on the gauge coupling of the form

$$\alpha_x \lesssim \{0.35, 2.5\} \times 10^{-6} \left( \frac{m_\psi}{\text{GeV}} \right)^{3/2}, \quad (34)$$

where the two numbers in brackets correspond to the analyses of Refs. [37] and [39], respectively. While the limit derived in Ref. [37] is considerably stronger, Ref. [39] (and Ref. [54]) argue for a weaker one based on the application of the ellipticity constraint only at larger galactic radii and a number of smaller factors. We show both upper bounds on  $\alpha_x$  in Figs. (4). These favor smaller temperature ratios  $\xi$  and larger DM masses  $m_\psi$ , well above the weak scale.

The limits on  $\alpha_x$  from the ellipticity of NGC720 correspond to an effective transfer cross section per mass below about  $\sigma_T/m_\psi \lesssim 1 \text{ cm}^2/\text{g}$  in this system with a velocity dispersion on the order

of  $v \simeq 300$  km/s. Dark matter self-interactions in this regime are described by a Rutherford-like transfer cross section [37, 39, 54]:

$$\sigma_T \simeq \frac{8\pi \alpha_x^2}{m_\psi^2} \frac{1}{v^4} \ln \Lambda, \quad (35)$$

where  $\ln \Lambda \sim 45 - 75$  is a collinear enhancement factor cut off by the typical interparticle spacing in the system [39]. Since this cross section has a very strong velocity dependence, the DM self-interactions in systems with lower velocity dispersions such as dwarf halos can be much stronger. Using typical velocities and densities for dwarf halos, this translates into

$$\sigma_T/m_\psi \simeq 18 \text{ cm}^2/\text{g} \left(\frac{\alpha_x}{0.1}\right)^2 \left(\frac{5 \times 10^4 \text{ GeV}}{m_\psi}\right)^3 \left(\frac{10 \text{ km/s}}{v}\right)^4 \left(\frac{\ln \Lambda}{50}\right) \quad (36)$$

Interaction cross sections of this size are expected to lead to the formation of cores in dwarf halos, with Refs. [55, 56] suggesting a better agreement between simulations and data for  $\sigma_T/m_\psi \sim 10 \text{ cm}^2/\text{g}$ . On the other hand, it is not clear what the upper bound on  $\sigma_T/m_\psi$  is from these systems, with the simulations of Ref. [57] finding reasonable behavior for  $\sigma_T/m_\psi = 50 \text{ cm}^2/\text{g}$  (the largest value studied) and Ref. [39] arguing that much larger values can work as well. Indeed, the results of Ref. [57] appear to be consistent with the approximate duality between  $\sigma_T/m_\psi$  and  $m_\psi/\sigma_T$  about Knudsen number close to unity suggested in Ref. [39] based on the analyses of Refs. [58, 59]. For reference, we also show dashed contours indicating  $\sigma_T/m_\psi = 10 \text{ cm}^2/\text{g}$  in Figs. 4.

## V. CONCLUSIONS

The standard expectation for non-renormalizable operators in the early universe is that their effects are greatest at high temperatures and that they decouple at lower temperatures. For this reason, DM creation from SM collisions connecting to a secluded dark sector through a non-renormalizable operator is referred to as UV freeze-in [10, 22]. In this work we showed that such operators can also contribute importantly at lower temperatures when combined with freeze-out in a dark sector.

To illustrate the effect, we studied a simple dark sector consisting of a massive Dirac fermion  $\psi$  DM candidate and a massless Abelian dark vector  $X^\mu$ , with the only connection to the SM through the dimension-five fermionic Higgs portal operator of Eq. (1). At the end of reheating, the dark sector can be populated by transfer reactions  $\text{SM} + \text{SM} \rightarrow \psi + \bar{\psi}$  mediated by the non-renormalizable portal operator to a density below the value it would have in full equilibrium with the SM. As the universe cools further, the population of dark fermions can equilibrate with the dark vectors at temperature  $T_x$  below the visible SM temperature  $T$  provided the dark gauge coupling and the initial fermion density are large enough. Freeze-out occurs in the dark sector when  $T_x$  falls below the fermion mass  $m_\psi$ . For a broad range of parameters in this theory, the relic density of  $\psi$  fermions can receive a significant additional enhancement from late transfer reactions through the non-renormalizable portal operator during the course of the freeze-out process for  $T$  down and below the fermion mass. The UV connector operator of Eq. (1) is therefore seen to play an important role in the IR.

The simple dark sector theory we considered also has interesting implications for DM self-interactions, which are motivated by a number of puzzles in cosmic structure [48, 49]. Such interactions were investigated for this theory in Refs. [37, 39, 54] and suggest that to be viable larger DM masses and smaller temperature ratios  $\xi = T_x/T$  are required to avoid bounds from the observed ellipticity of NG720. These bounds, and the dependence of the self-interaction cross section on the DM velocity, could potentially be softened by extending the theory to include a small mass for the dark vector [51]. The calculations presented in this work can be carried over to such a massive vector scenario provided its mass is much smaller than the decoupling temperature of the dark fermion so that it provides a relativistic thermal bath during this process. Furthermore, the vector mass would also have to be small enough to avoid too much vector boson DM [60, 61].

While this work focused on a specific dark sector theory and non-renormalizable connector operator, a similar IR contribution from a non-renormalizable connector to the density of dark-sector DM is expected to occur as well for other dark sectors or connector operators. For the effect to arise, the DM candidate in the dark sector must undergo significant annihilation to allow the power-suppressed transfer reactions (relative to reheating) of the connector operator to catch up. Other non-renormalizable connector operators can also lead to late IR transfer contributions to the DM relic density, although initial estimates suggest that the effect becomes less important as the operator dimension increases. Late-time transfer of a symmetric density could also be relevant in scenarios of secluded asymmetric DM.

Dark matter arising from a dark sector that is colder than the SM in the early universe has been investigated in a wide range of scenarios of new physics [19, 22, 37–39, 62–73]. In some of these works, the dark temperature  $T_x$  is taken as an input to the calculation of the DM relic density without reference to how the dark sector was populated initially. Our results show that such an assumption is not always justified, and the nature of the connector operators that mediate transfer from the SM to the dark sector can play an important role in determining the relic density of DM.

## ACKNOWLEDGEMENTS

We thank Dave McKeen, Nirmal Raj, Kris Sigurdson, Sean Tulin, Graham White, and Yue Zhang for helpful discussions. DEM acknowledges the Aspen Center for Physics, which is funded by National Science Foundation grant PHY-1607611, for their hospitality while this work was being completed. This work is supported by the Natural Sciences and Engineering Research Council of Canada (NSERC), with DEM supported in part by Discovery Grants and LF by a CGS D scholarship. TRIUMF receives federal funding via a contribution agreement with the National Research Council of Canada.

## Appendix A: Calculation of Transfer Rates

In this appendix we calculate the effective transfer rates of number and energy density from the visible sector to the dark sector through the operator of Eq. (1). The squared matrix element for  $\psi + \bar{\psi} \rightarrow H + H^\dagger$  derived from this interaction and summed over both initial and final degrees of

freedom is

$$|\widetilde{\mathcal{M}}|^2 = \frac{4}{M^2}(s - 4m_\psi^2) , \quad (\text{A1})$$

with  $s = (p_1 + p_2)^2$ . Note that we assume implicitly that the Higgs is in the electroweak unbroken phase and can be treated as a massless  $SU(2)_L$  scalar doublet.

### 1. Number Transfer

The relevant number transfer term via  $\psi(1) + \bar{\psi}(2) \rightarrow H(3) + H^\dagger(4)$  is

$$\begin{aligned} \mathcal{T}(T) &\equiv \langle \sigma_{tr} v(T) \rangle (n_\psi^2 - n_{\psi,eq}^2(T)) \\ &\equiv \int d\Pi_1 \int d\Pi_2 \int d\Pi_3 \int d\Pi_4 (2\pi)^4 \delta^{(4)}(p_i) |\widetilde{\mathcal{M}}|^2 (f_1 f_2 - f_3 f_4) , \end{aligned} \quad (\text{A2})$$

where  $d\Pi_i = d^3 p_i / 2E_i (2\pi)^3$ . To make the calculation tractable, we approximate the distribution functions by the Maxwell-Boltzmann form  $f_i = \zeta_i e^{-E_i/T}$ , where  $\zeta_i$  is the rescaling needed to get the correct number densities relative to equilibrium at temperature  $T$ . We expect that the Maxwell-Boltzmann approximation used here is correct up to factors very close to unity.

For  $n_\psi \ll n_{\psi,eq}(T)$  we have  $f_1 = f_2 \simeq 0$ , while Higgs fields in full thermodynamic equilibrium with the SM (in the electroweak unbroken phase) imply  $f_3 = f_4 = 1$ . The transfer term then reduces to

$$\mathcal{T}(T) = \int d\Pi_1 \int d\Pi_2 (4g_\psi^2 E_1 E_2 \sigma_{tr} v) e^{-(E_1 + E_2)/T} , \quad (\text{A3})$$

with  $g_\psi = 2$  being the number of fermion spin states. Note that the combination in brackets is Lorentz invariant and can depend only on the variable  $s$ . It is given by

$$\begin{aligned} (4g_\psi^2 E_1 E_2 \sigma_{tr} v) &= \int d\Pi_3 \int d\Pi_4 (2\pi)^4 \delta^{(4)}(p_i) |\widetilde{\mathcal{M}}|^2 \\ &= \frac{1}{8\pi} \left( \frac{1}{4\pi} \int d\Omega |\widetilde{\mathcal{M}}|^2 \right)_{CM} \\ &= \frac{1}{2\pi} \frac{1}{M^2} (s - 4m_\psi^2) . \end{aligned} \quad (\text{A4})$$

To integrate this over the initial states, we follow Refs. [46, 47] and use the fact that the integrand depends only on  $s$  and  $E_+ = (E_1 + E_2)$  to write

$$\int d\Pi_1 \int d\Pi_2 = \frac{1}{4(2\pi)^4} \int_{4m_\psi^2}^{\infty} ds \int_{\sqrt{s}}^{\infty} dE_+ \sqrt{1 - 4m_\psi^2/s} \sqrt{E_+^2 - s} . \quad (\text{A5})$$



Since the only  $E_+$  dependence of the integrand is in the Boltzmann exponential, integrating using a Bessel function identity<sup>5</sup> gives

$$\begin{aligned}\mathcal{T}(T) &= \frac{1}{4(2\pi)^4} \int_{4m_\psi^2}^{\infty} ds (4g_1g_2E_1E_2\sigma_{tr}v) \sqrt{1 - 4m_\psi^2/s} \\ &= \frac{1}{2(2\pi)^5} \frac{T^6}{M^2} \mathcal{F}(x),\end{aligned}\tag{A6}$$

where  $x = m_\psi/T$  and

$$\begin{aligned}\mathcal{F}(x) &= \int_{2x}^{\infty} du u (u^2 - 4x^2)^{3/2} K_1(u) \\ &\simeq \begin{cases} 16 & ; \quad x \ll 1 \\ 6\pi x^2 e^{-2x} & ; \quad x \gg 1 \end{cases}\end{aligned}\tag{A7}$$

## 2. Energy Transfer

We are also interested in the net rate of energy transfer between the visible and dark sectors. The relevant energy collision term for  $\psi + \bar{\psi} \rightarrow H + H^\dagger$  is identical to Eq. (A2) but with an additional factor of  $\Delta E = (E_1 + E_2) = E_+$  in the integrand. The result is<sup>6</sup>

$$\begin{aligned}\mathcal{U}(T) &\equiv \langle \Delta E \cdot \sigma_{tr}v(T) \rangle (n_\psi^2 - n_{\psi,eq}^2(T)) \\ &\equiv \frac{T}{4(2\pi)^4} \int_{4m_\psi^2}^{\infty} ds (4g_1g_2E_1E_2\sigma_{tr}v) \sqrt{s - 4m_\psi^2} \sqrt{s} K_2(\sqrt{s}/T) \\ &= \frac{1}{2(2\pi)^5} \frac{T^7}{M^2} \mathcal{G}(x)\end{aligned}\tag{A8}$$

with  $x = m_\psi/T$  and

$$\begin{aligned}\mathcal{G}(x) &= \int_{2x}^{\infty} du u^2 (u^2 - 4x^2)^{3/2} K_2(u) \\ &\simeq \begin{cases} 96 & ; \quad x \ll 1 \\ 12\pi x^3 e^{-2x} & ; \quad x \gg 1 \end{cases}\end{aligned}\tag{A9}$$

---

[1] N. Aghanim *et al.* (Planck), (2018), arXiv:1807.06209 [astro-ph.CO].

<sup>5</sup>  $K_\nu(z) = \frac{\sqrt{\pi}z^\nu}{2^\nu\Gamma(\nu+1/2)} \int_1^\infty dt (t^2 - 1)^{\nu-1/2} e^{-zt}$ .

<sup>6</sup>  $\int_1^\infty dt t \sqrt{t^2 - 1} e^{-zt} = -\frac{d}{dz} [K_1(z)/z] = K_2(z)/z$ .

- [2] G. Jungman, M. Kamionkowski, and K. Griest, Phys. Rept. **267**, 195 (1996), arXiv:hep-ph/9506380 [hep-ph].
- [3] G. Bertone, D. Hooper, and J. Silk, Phys. Rept. **405**, 279 (2005), arXiv:hep-ph/0404175 [hep-ph].
- [4] M. Lisanti, in *Proceedings, Theoretical Advanced Study Institute in Elementary Particle Physics: New Frontiers in Fields and Strings (TASI 2015): Boulder, CO, USA, June 1-26, 2015* (2017) pp. 399–446, arXiv:1603.03797 [hep-ph].
- [5] S. Wolfram, Phys. Lett. **82B**, 65 (1979).
- [6] R. J. Scherrer and M. S. Turner, Phys. Rev. **D33**, 1585 (1986), [Erratum: Phys. Rev.D34,3263(1986)].
- [7] E. W. Kolb and M. S. Turner, Front. Phys. **69**, 1 (1990).
- [8] P. S. Bhupal Dev, A. Mazumdar, and S. Qutub, Front.in Phys. **2**, 26 (2014), arXiv:1311.5297 [hep-ph].
- [9] H. Baer, K.-Y. Choi, J. E. Kim, and L. Roszkowski, Phys. Rept. **555**, 1 (2015), arXiv:1407.0017 [hep-ph].
- [10] L. J. Hall, K. Jedamzik, J. March-Russell, and S. M. West, JHEP **03**, 080 (2010), arXiv:0911.1120 [hep-ph].
- [11] J. McDonald, Phys. Rev. Lett. **88**, 091304 (2002), arXiv:hep-ph/0106249 [hep-ph].
- [12] C. Cheung, G. Elor, L. J. Hall, and P. Kumar, JHEP **03**, 042 (2011), arXiv:1010.0022 [hep-ph].
- [13] C. Cheung, G. Elor, L. J. Hall, and P. Kumar, JHEP **03**, 085 (2011), arXiv:1010.0024 [hep-ph].
- [14] X. Chu, T. Hambye, and M. H. G. Tytgat, JCAP **1205**, 034 (2012), arXiv:1112.0493 [hep-ph].
- [15] C. E. Yaguna, JHEP **08**, 060 (2011), arXiv:1105.1654 [hep-ph].
- [16] C. E. Yaguna, JCAP **1202**, 006 (2012), arXiv:1111.6831 [hep-ph].
- [17] M. Blennow, E. Fernandez-Martinez, and B. Zaldivar, JCAP **1401**, 003 (2014), arXiv:1309.7348 [hep-ph].
- [18] M. Heikinheimo, T. Tenkanen, K. Tuominen, and V. Vaskonen, Phys. Rev. **D94**, 063506 (2016), [Erratum: Phys. Rev.D96,no.10,109902(2017)], arXiv:1604.02401 [astro-ph.CO].
- [19] G. Krnjaic, JHEP **10**, 136 (2018), arXiv:1711.11038 [hep-ph].
- [20] M. J. Baker, M. Breitbach, J. Kopp, and L. Mitnacht, JHEP **03**, 114 (2018), arXiv:1712.03962 [hep-ph].
- [21] N. Bernal, M. Heikinheimo, T. Tenkanen, K. Tuominen, and V. Vaskonen, Int. J. Mod. Phys. **A32**, 1730023 (2017), arXiv:1706.07442 [hep-ph].
- [22] F. Elahi, C. Kolda, and J. Unwin, JHEP **03**, 048 (2015), arXiv:1410.6157 [hep-ph].
- [23] S. B. Roland, B. Shakya, and J. D. Wells, Phys. Rev. **D92**, 113009 (2015), arXiv:1412.4791 [hep-ph].
- [24] J. McDonald, JCAP **1608**, 035 (2016), arXiv:1512.06422 [hep-ph].
- [25] S.-L. Chen and Z. Kang, JCAP **1805**, 036 (2018), arXiv:1711.02556 [hep-ph].
- [26] M. Garny, A. Palessandro, M. Sandora, and M. S. Sloth, (2018), arXiv:1810.01428 [hep-ph].
- [27] H. Pagels and J. R. Primack, Phys. Rev. Lett. **48**, 223 (1982).
- [28] J. R. Ellis, D. V. Nanopoulos, and S. Sarkar, Nucl. Phys. **B259**, 175 (1985).
- [29] V. S. Berezinsky, Phys. Lett. **B261**, 71 (1991).
- [30] T. Moroi, H. Murayama, and M. Yamaguchi, Phys. Lett. **B303**, 289 (1993).
- [31] A. DiFranzo, P. J. Fox, and T. M. P. Tait, JHEP **04**, 135 (2016), arXiv:1512.06853 [hep-ph].
- [32] L. Lopez-Honorez, T. Schwetz, and J. Zupan, Phys. Lett. **B716**, 179 (2012), arXiv:1203.2064 [hep-ph].
- [33] A. De Simone, G. F. Giudice, and A. Strumia, JHEP **06**, 081 (2014), arXiv:1402.6287 [hep-ph].
- [34] M. A. Fedderke, J.-Y. Chen, E. W. Kolb, and L.-T. Wang, JHEP **08**, 122 (2014), arXiv:1404.2283 [hep-ph].
- [35] P. Adshead, Y. Cui, and J. Shelton, JHEP **06**, 016 (2016), arXiv:1604.02458 [hep-ph].
- [36] E. Hardy and J. Unwin, JHEP **09**, 113 (2017), arXiv:1703.07642 [hep-ph].
- [37] J. L. Feng, H. Tu, and H.-B. Yu, JCAP **0810**, 043 (2008), arXiv:0808.2318 [hep-ph].
- [38] S. Das and K. Sigurdson, Phys. Rev. **D85**, 063510 (2012), arXiv:1012.4458 [astro-ph.CO].
- [39] P. Agrawal, F.-Y. Cyr-Racine, L. Randall, and J. Scholtz, JCAP **1705**, 022 (2017), arXiv:1610.04611 [hep-ph].
- [40] M. Pospelov, A. Ritz, and M. B. Voloshin, Phys. Lett. **B662**, 53 (2008), arXiv:0711.4866 [hep-ph].
- [41] J. Hisano, S. Matsumoto, and M. M. Nojiri, Phys. Rev. Lett. **92**, 031303 (2004), arXiv:hep-ph/0307216 [hep-ph].
- [42] J. Hisano, S. Matsumoto, M. M. Nojiri, and O. Saito, Phys. Rev. **D71**, 063528 (2005), arXiv:hep-ph/0412403 [hep-ph].

- [43] M. Cirelli, A. Strumia, and M. Tamburini, Nucl. Phys. **B787**, 152 (2007), arXiv:0706.4071 [hep-ph].
- [44] M. Pospelov and A. Ritz, Phys. Lett. **B671**, 391 (2009), arXiv:0810.1502 [hep-ph].
- [45] B. von Harling and K. Petraki, JCAP **1412**, 033 (2014), arXiv:1407.7874 [hep-ph].
- [46] P. Gondolo and G. Gelmini, Nucl. Phys. **B360**, 145 (1991).
- [47] J. Edsjo and P. Gondolo, Phys. Rev. **D56**, 1879 (1997), arXiv:hep-ph/9704361 [hep-ph].
- [48] D. N. Spergel and P. J. Steinhardt, Phys. Rev. Lett. **84**, 3760 (2000), arXiv:astro-ph/9909386 [astro-ph].
- [49] S. Tulin and H.-B. Yu, Phys. Rept. **730**, 1 (2018), arXiv:1705.02358 [hep-ph].
- [50] L. Ackerman, M. R. Buckley, S. M. Carroll, and M. Kamionkowski, *Proceedings, 7th International Heidelberg Conference on Dark Matter in Astro and Particle Physics (DARK 2009): Christchurch, New Zealand, January 18-24, 2009*, Phys. Rev. **D79**, 023519 (2009), [,277(2008)], arXiv:0810.5126 [hep-ph].
- [51] S. Tulin, H.-B. Yu, and K. M. Zurek, Phys. Rev. **D87**, 115007 (2013), arXiv:1302.3898 [hep-ph].
- [52] D. A. Buote, T. E. Jeltema, C. R. Canizares, and G. P. Garmire, Astrophys. J. **577**, 183 (2002), arXiv:astro-ph/0205469 [astro-ph].
- [53] P. J. Humphrey, D. A. Buote, C. R. Canizares, A. C. Fabian, and J. M. Miller, Astrophys. J. **729**, 53 (2011), arXiv:1010.6078 [astro-ph.CO].
- [54] F. Kahlhoefer, K. Schmidt-Hoberg, M. T. Frandsen, and S. Sarkar, Mon. Not. Roy. Astron. Soc. **437**, 2865 (2014), arXiv:1308.3419 [astro-ph.CO].
- [55] M. Vogelsberger, J. Zavala, and A. Loeb, Mon. Not. Roy. Astron. Soc. **423**, 3740 (2012), arXiv:1201.5892 [astro-ph.CO].
- [56] J. Zavala, M. Vogelsberger, and M. G. Walker, Mon. Not. Roy. Astron. Soc. **431**, L20 (2013), arXiv:1211.6426 [astro-ph.CO].
- [57] O. D. Elbert, J. S. Bullock, S. Garrison-Kimmel, M. Rocha, J. Oorbe, and A. H. G. Peter, Mon. Not. Roy. Astron. Soc. **453**, 29 (2015), arXiv:1412.1477 [astro-ph.GA].
- [58] K. Ahn and P. R. Shapiro, *2nd Korean Astrophysics Workshop on Formation and Interaction of Galaxies Pohang, Korea, June 24-27, 2002*, J. Korean Astron. Soc. **36**, 89 (2003), arXiv:astro-ph/0212575 [astro-ph].
- [59] K.-J. Ahn and P. R. Shapiro, Mon. Not. Roy. Astron. Soc. **363**, 1092 (2005), arXiv:astro-ph/0412169 [astro-ph].
- [60] E. Ma, Phys. Lett. **B772**, 442 (2017), arXiv:1704.04666 [hep-ph].
- [61] M. Duerr, K. Schmidt-Hoberg, and S. Wild, JCAP **1809**, 033 (2018), arXiv:1804.10385 [hep-ph].
- [62] A. E. Faraggi and M. Pospelov, Astropart. Phys. **16**, 451 (2002), arXiv:hep-ph/0008223 [hep-ph].
- [63] F.-Y. Cyr-Racine and K. Sigurdson, Phys. Rev. **D87**, 103515 (2013), arXiv:1209.5752 [astro-ph.CO].
- [64] K. K. Boddy, J. L. Feng, M. Kaplinghat, and T. M. P. Tait, Phys. Rev. **D89**, 115017 (2014), arXiv:1402.3629 [hep-ph].
- [65] K. K. Boddy, J. L. Feng, M. Kaplinghat, Y. Shadmi, and T. M. P. Tait, Phys. Rev. **D90**, 095016 (2014), arXiv:1408.6532 [hep-ph].
- [66] A. Berlin, D. Hooper, and G. Krnjaic, Phys. Lett. **B760**, 106 (2016), arXiv:1602.08490 [hep-ph].
- [67] A. Berlin, D. Hooper, and G. Krnjaic, Phys. Rev. **D94**, 095019 (2016), arXiv:1609.02555 [hep-ph].
- [68] A. Soni and Y. Zhang, Phys. Rev. **D93**, 115025 (2016), arXiv:1602.00714 [hep-ph].
- [69] L. Forestell, D. E. Morrissey, and K. Sigurdson, Phys. Rev. **D95**, 015032 (2017), arXiv:1605.08048 [hep-ph].
- [70] J. Halverson, B. D. Nelson, and F. Ruehle, Phys. Rev. **D95**, 043527 (2017), arXiv:1609.02151 [hep-ph].
- [71] B. S. Acharya, M. Fairbairn, and E. Hardy, JHEP **07**, 100 (2017), arXiv:1704.01804 [hep-ph].
- [72] L. Forestell, D. E. Morrissey, and K. Sigurdson, Phys. Rev. **D97**, 075029 (2018), arXiv:1710.06447 [hep-ph].
- [73] N. Bernal, M. Dutra, Y. Mambrini, K. Olive, M. Peloso, and M. Pierre, Phys. Rev. **D97**, 115020 (2018), arXiv:1803.01866 [hep-ph].